Relation between Direction-of-Arrival distribution of reflected sounds in late reverberation and room characteristics: Geometrical acoustics investigation

Yuto Izumi[a], Makoto Otani[a]

[a] *Graduate School of Engineering, Kyoto University, Japan*

Abstract

It has been reported that Direction-of-Arrival (DoA) distribution of reflected sounds is not isotropic in late reverberation. However, it is not clear how room characteristics contribute to the anisotropic DoA distribution. In this paper, the relation between DoA distribution in late reverberation and room characteristics is analyzed by using geometrical acoustic simulation and plane wave decomposition. The computational results showed that the DoA distribution in late reverberation is biased depending on the arrangement of absorptive surfaces and the shape of the room while the source position does not have prominent effects.

Keywords: Direction-of-Arrival, late reverberation, plane wave decomposition, decay cancellation

1. Introduction

In auditory perception in room acoustics, Direction-of-Arrivals (DoA) of reflected sounds is one of the important factors because it has prominent effects on spatial impression of sound sources and an acoustic field, such as auditory source width (ASW) [1] and listener envelopment (LEV) [2, 3]. However, for late reverberation, diffuse sound field is often assumed. Actually, classical theories of reverberation [4, 5] assume perfectly diffuse field, in which DoA of reflected sound is assumed to be isotropic at any position in the sound field. However, actual sound field can never be perfectly diffuse.

Recent studies have reported that DoA distribution of late reverberation is not isotropic in real measurements using C-C method [6, 7] or plane wave decomposition [8, 9]. In late reverberation, many sound waves arrive simultaneously or at very close intervals. While a lot of microphones are required for plane wave decomposition, it is able to estimate the DoAs of multiple soud waves that arrive simultaneously from different directions. The authors also have proposed a method for DoA distribution using plane wave decomposition and decay cancellation [10]. In [10], real measurements were performed in a multipurpose hall, and the DoA analysis showed that DoA distribution of late reverberation is anisotropic at any frequency and any receiver position, which is more prominent as time passes.

However, it is not clear how anisotropic DoA distribution in late reverberation is characterized by physical properties including shape of a room, absorptive surface in a room, source position, and receiver position, while the real measurement and DoA analysis performed in [10] implies that the DoA distributions in late reverberation is affected by the acoustic absorption of the room.

In order to further explore what and how acoustic characteristics of the room and positions of source and receiver have an impact on the DoA distribution in late reverberation, this paper performs geometrical acoustic simulation which replicates the real measurement in the authors' previous study [10] and enables a parametric study with various absorption coefficients of surfaces in the room.

Section 2 describes a method for analyzing DoA distribution from spherical microphone array response based on the plane wave decomposition and decay cancellation. Section 3 briefly introduces the analysis result of the DoA distribution from the real measurements performed in a multipurpose hall. Section 4 demonstrates analysis results from geometrical acoustics simulation applied to a simplified model of the hall examined in Section 3. Sections 5 and 6 respectively discusses and concludes the results obtained in the current study.

2. Method

2.1. Plane wave decomposition

Plane wave decomposition is a method to represent the sound field as a superposition of plane waves, which is used to estimate DoA [11, 12, 13, 14]. In the following, plane wave decomposition is introduced according to [11].

Consider the sound pressure of a unit-amplitude plane wave which arrives from the direction (θ_l, ϕ_l) with the wave number k. The sound pressure observed at (θ, ϕ, r) is given by

$$p_l(\theta, \phi, r) = \sum_{n=0}^{\infty} \sum_{m=-n}^{n} b_n(kr) Y_n^m(\theta, \phi) Y_n^{m*}(\theta_l, \phi_l), \tag{1}$$

where $Y_n^m(\phi, \theta)$ is spherical harmonics function with the degree n and order m, and for an open spherical array, $b_n(kr)$ is

$$b_n(kr) = 4\pi i^n j_n(kr), \tag{2}$$

where $i = \sqrt{-1}$, and j_n is the n-th order spherical Bessel function.

Assuming that the sound field is composed by an infinite number of plane waves, the sound pressure observed at (θ, ϕ) can be written as

$$p(\theta, \phi, r) = \int_{\Omega_l \in S^2} w_l p_l(\theta, \phi, r) d\Omega_l, \tag{3}$$

where w_l is the plane wave coefficients. The spherical harmonics decomposition of $p(\theta, \phi, r)$ can be written as

$$p(\theta, \phi, r) = \sum_{n=0}^{\infty} \sum_{m=-n}^{n} p_{nm} Y_n^m(\theta, \phi). \tag{4}$$

Using Eqs. (1), (4), and the spherical harmonics decomposition of w_l, w_l can be written as

$$w_l = \sum_{n=0}^{\infty} \sum_{m=-n}^{n} \frac{p_{nm}}{b_n(kr)} Y_n^m(\theta_l, \phi_l). \tag{5}$$

Here, w_l represents the amplitude and phase of the plane wave arriving from the direction (θ_l, ϕ_l). Therefore, the DoA distribution can be estimated from this equation.

2.1.1. Truncation order

In most practical situations, w_l is calculated from the following formula:

$$w_l = \sum_{n=0}^{N} \sum_{m=-n}^{n} \frac{p_{nm}}{b_n(kr)} Y_n^m(\theta_l, \phi_l), \tag{6}$$

where N is the truncation order. In case that the microphones are distributed equally, to ensure a truncation of spherical harmonics decompositions to N, it is necessary to use M microphones, where [15]:

$$M \geq (N+1)^2 \tag{7}$$

and the spatial resolution ψ_0 [rad] is given by

$$2\psi_0 \simeq 2\pi/N \tag{8}$$

The radial function b_n, Eq. (2), are plotted in Fig. 1, demonstrating that the amplitude approaches to zero as the order of $b_n(kr)$ increases when kr is small. To prevent divergence of $1/b_n(kr)$ in Eq. (6), $b_n \gg 0$ is required. Moreover, in order to avoid the spatial aliasing, the upper frequency is limited by $kr < N$.

From the reasons mentioned above, the upper and lower limits of frequency and the truncation order N are restricted due to the number of microphone M and the radius of the microphone array r.

2.2. Decay cancellation

In this paper, we take an average of amplitudes of the plane waves in each direction over time for a period of interest, such as from 80 ms to 160 ms after the direct sound arrives, in order to analyze DoA distribution in late reverberation. However, the results would be affected more by earlier part in the time windows because the amplitude generally attenuates as time passes. Then we introduce decay cancellation [16].

Consider the decay cancellation of the impulse response $p(t)$. The decay curve $E_s(t)$ of $p(t)$ is given by

$$E_s(t) = \int_t^\infty p(\tau)^2 d\tau. \tag{9}$$

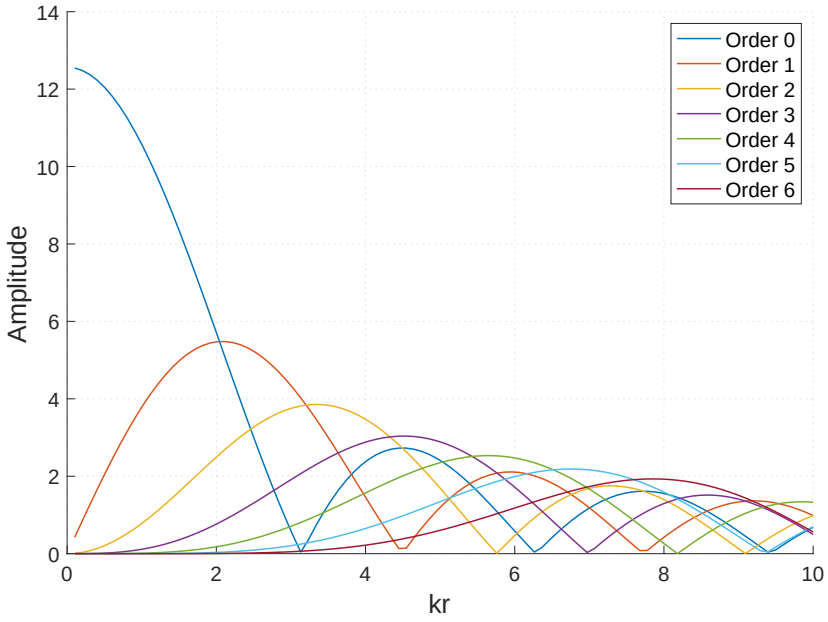

Figure 1: Amplitude of $b_n(kr)$

Then the decay-cancelled impulse response $g(t)$ is defined as

$$g(t) = \frac{p(t)}{\sqrt{E_s(t)}}. \tag{10}$$

3. Measurement analysis

In this section, the results of the analysis from real measurements in a multipurpose hall [10] is introduced.

3.1. Measurement set

A spherical rigid microphone array, with 64 omnidirectional microphones arranged equally on a sphere based on Fibonacci-spiral [17] and 50 mm radius, was used in this measurement. Impulse response was measured in a multipurpose hall, Hardy Hall in Doshisha University, Japan. The positions of the loudspeaker (Genelec, 1037C) and the microphone array are arranged, which are shown as S1 and R, respectively, in the simplified hall model, illustrated in Fig. 2. The samping frequency was 48,000 Hz.

3.2. Procedure

In the first step, the impulse responses measured using a spherical microphone array were converted to time-frequency domain by using short time Fourier transform (STFT). Here, 256-samples Hanning window with 50-samples overlapping was applied. Next, plane wave decomposition was applied to the signals. Third, the distance decay was canceled by using decay cancellation. In the decay cancellation, the decay curve in Eq. (10) was calculated by using the omnidirectional component of the signals obtained in the previous step. Finally, the signals were extracted for a period of interest and then averaged. The results are shown in color maps using Mollweide projection, where latitude and longitude correspond to elevation and azimuth, respectively; a direction of 0-degrees azimuth and 0-degrees elevation corresponds to frontal direction; the mark x represents the source direction. The results show the time transition of the DoA distributions with 80 ms time windows.

3.3. Measurement results

Figure 3 depicts the DoA distributions analyzed in the octave band with center frequency 4,000 Hz and truncation order $N = 4$. It can be found that the distributions are biased toward the frontal hemicircle in the horizontal plane with 0 degrees elevation after a certain period of time. The anisotropic DoA distribution is more prominent as time passes.

4. Simulation

Geometrical acoustic simulation was performed using CATT-Acoustic (9.1b, TUCT v2.0a). Figure 2 shows the model including the positions of the sound sources (S1, S2, and S3) and the receiver (R). A spherical open microphone array, with 64 omnidirectional microphones arranged equally on a sphere of 50 mm radius based on Fibonacci-spiral [17], was assumed in this simulation. Omnidirectional sound sources were arranged at S1, S2, and S3, whose relative positions from the receiver were (13.0, -1.25, 0.0), (-3.25, -6.25, 2.0), (0.75, 1.25,

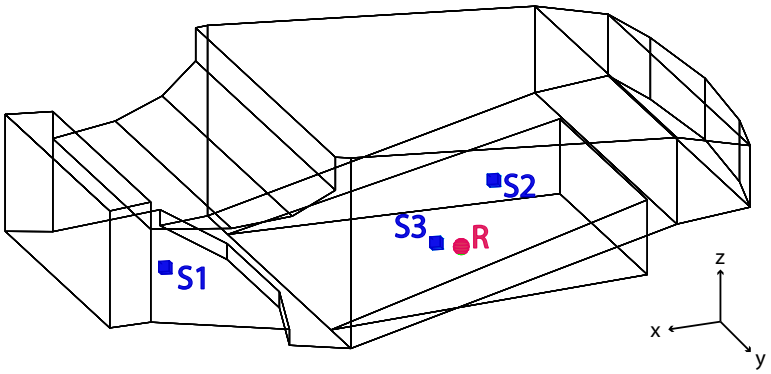

Figure 2: Computer model used for the geometrical acoustic simulation

0.0) m, with x axis corresponding to the front and y axis corresponding to the left. The sampling frequency was 48,000 Hz. The acoustic absorption coefficient of each surface was set according to Table 1, and was constant regardless of frequency. The scattering coefficient of each surface was 0 at all conditions, and the calculation was performed with Algorithm 1 [18].

The calculated impulse responses were analyzed in the same way as the measured impulse responses in Section 3. For the reasons mentioned in Sec. 2.1.1, we analyze the DoA distributions in the octave band with center frequencies 1,000, 2,000, and 4,000 Hz and truncation order $N = 2$, 2, and 4, respectively.

5. Results

Figures 4 - 10 depict the simulation results. The DoA distribution is analyzed in the octave band with center frequency of 4,000 Hz and truncation order $N = 4$. The truncation order $N = 4$ was set to prevent divergence of $1/b_n(kr)$ in Eq. (6). The scale of the colormap is normalized to the mean value.

5.1. Inhomogeneous absorption

Figure 4 demonstrates that in condition A in which the acoustic absorption coefficient of the floor is high (0.8), the DoA distribution in late reverberation

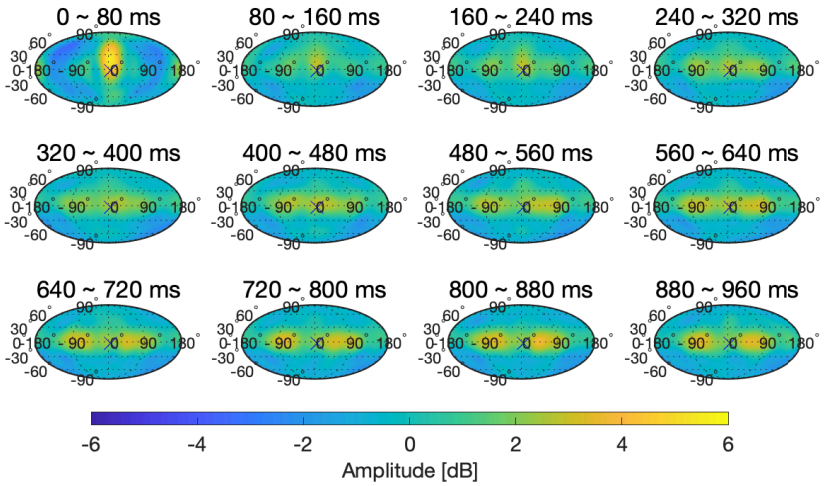

Figure 3: Measurement results (4,000 Hz)

is biased toward 0 degrees elevation.

Figure 5 illustrates that in condition B in which the acoustic absorption coefficient of the ceiling is high (0.8), the DoA distribution is also biased toward 0 degrees; however, the direction in which the energy of reverberation is concentrated is slightly higher than case A

Figure 6 shows that in condition C in which the left wall has a high acoustic absorption coefficient (0.8), the DoA distribution is biased toward the front of the median plane.

5.2. Homogeneous absorption

Figure 7 shows that the DoA distribution is biased toward 0 degrees elevation in condition D in which the acoustic absorption coefficients of all surfaces are 0.2. Compared to conditions A and B, the bias is weak.

Figure 8 shows that the DoA distribution is almost isotropic in condition E in which the acoustic absorption coefficients of all surfaces are 0.

Condition	Floor	Ceiling	Left wall	Right wall	Source
A	0.8	0.2	0.2	0.2	S1
B	0.2	0.8	0.2	0.2	S1
C	0.2	0.2	0.8	0.2	S1
D	0.2	0.2	0.2	0.2	S1
E	0	0	0	0	S1
F	0.8	0.2	0.2	0.2	S2
G	0.8	0.2	0.2	0.2	S3

Table 1: Acoustic absorption coefficient in the simulation

5.3. Effect of sound source position

From Figs. 9 and 10, it can be seen that the DoA distribution in late reverberation basically does not change when the sound source position changes. The DoA distribution is still biased toward 0 degrees elevation. Even when the sound source is close to the receiver, the DoA distribution hardly changed.

6. Discussion

6.1. Comparison between measurement and simulation

There are upholstered seats which have high absorption coefficient on the floor in the hall; that is, the acoustic absorption coefficients of condition A is similar to those in the real measurement. Comparing Figs. 3 and 4, it can be found that the DoA distribution of condition A in the late reverberation are similar to that of the real measurement, suggesting that the current simulation is valid.

The DoA distribution in late reverberation is biased when the acoustic absorption coefficient for a surface is higher than the others. On the other hand, the DoA distribution in late reverberation is almost isotropic when the acoustic sound coefficients for all surfaces are 0. In other words, the sound field is almost diffused when all surfaces do not absorb sound. These results suggest that reflections in late reverberation arrive almost equally from all directions,

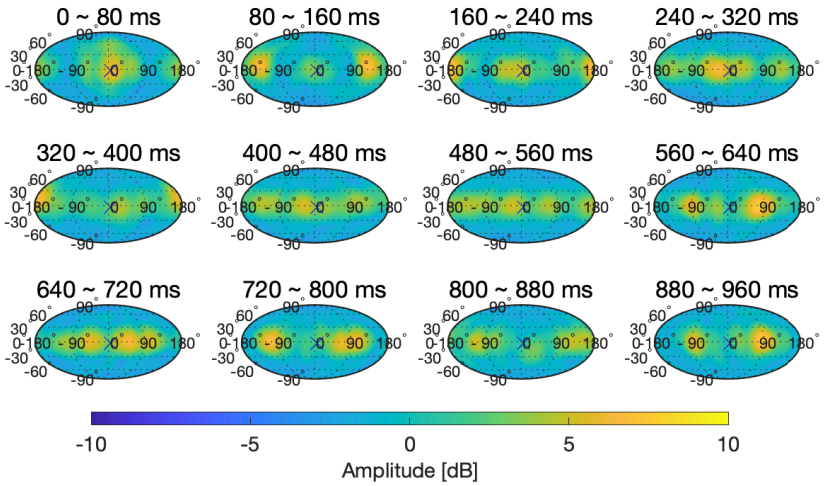

Figure 4: Condition A (Acoustic coefficient for the floor surface: 0.8, and that for the other surface: 0.2, Sound source position: S1)

but each reflection has different energy because of the acoustic absorption at each surface.

However, the DoA distribution is biased when the acoustic absorption coefficients for all surfaces are 0.2. This result implies that the shape of the room also affects the DoA distribution in late reverberation. The distance between the ceiling and the floor is shorter than the distance between the back wall of the stage and the rear wall of the hall (See Fig. 2). It is supposed that the sounds which are reflected repetedly among the ceiling and the floor are absorbed more than those in other propagation paths, and they attenuate faster than the others.

The comparison among source positions reveals that the source position does not lead to prominent variation in the DoA distributions. This implies that the DoA distribution in late reverberation does not depend on the sound source position.

The results suggest that the DoA distribution in late reverberation might

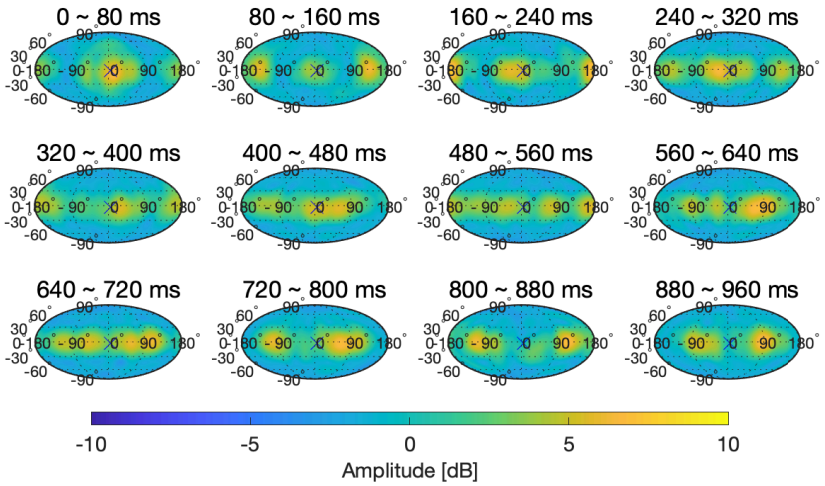

Figure 5: Condition B (Acoustic coefficient for the ceiling surface: 0.8, and that for the other surface: 0.2, Sound source position: S1)

be useful for analyzing acoustic characteristics of a room. By analyzing DoA distribution in late reverberation, it may be possible to roughly estimate acoustic characteristics of a room with one or several measurements.

6.2. Frequency dependence

Figures 11 and 12 show the DoA distribution for Condition A analized in the octave bands with center frequency of 1,000 and 2,000 Hz. The truncation order is 2 for both of them. The DoA distributions analized at 1,000 and 2,000 Hz are also biased towards 0 degrees elevation. Compared with Fig. 4 for the center frequency of 4,000 Hz, the DoA distributions of late reverberation are almost same even when analyzed at different frequencies. The cause of the slight difference between them is the directivity pattern varying with the truncation order.

For this simulation, the absorption coefficient was constant regardless of frequency. Therefore, it can be considered that DoA distribution in late reverberation does not depend on the frequency. It should be noted that the absorption

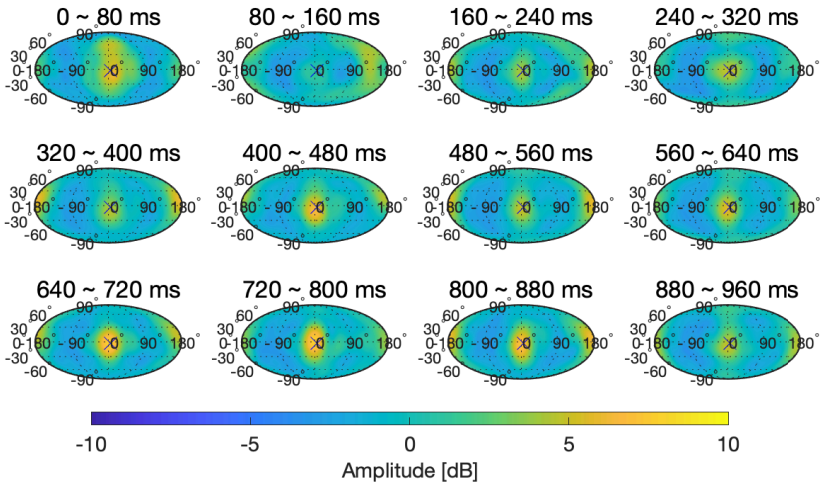

Figure 6: Condition C (Acoustic coefficient for the left wall surface: 0.8, and that for the other surface: 0.2, Sound source position: S1)

coefficients in actual environments are variable depending on frequencies, which lead to frequency-dependent DoA distribution.

6.3. Effect of decay cancellation

Figure 13 shows the results with and without decay cancellation for a case of 800-ms time window. Figure 13 depicts the DoA distribution for Condition A analized in the octave band with center frequency of 4,000 Hz without decay cancellation. Comparing Figs. 4 and 13, the analysis results are almost same. In this simulation, the time window length was 80-ms. The length of the time window is relatively short, thus, the effect of decay cancellation is limited.

Figure 14 demonstrates that, for 800-ms time window, the DoA distribution varies between the results with and without the decay cancellation; the influence of decay cancellation is more prominent in earlier time windows. This indicates that, in the room currently examined, the DoA distribution is more variable in the earlier part, which thereby yielding greater deviations between the results with and without the decay cancellation in earlier time windows.

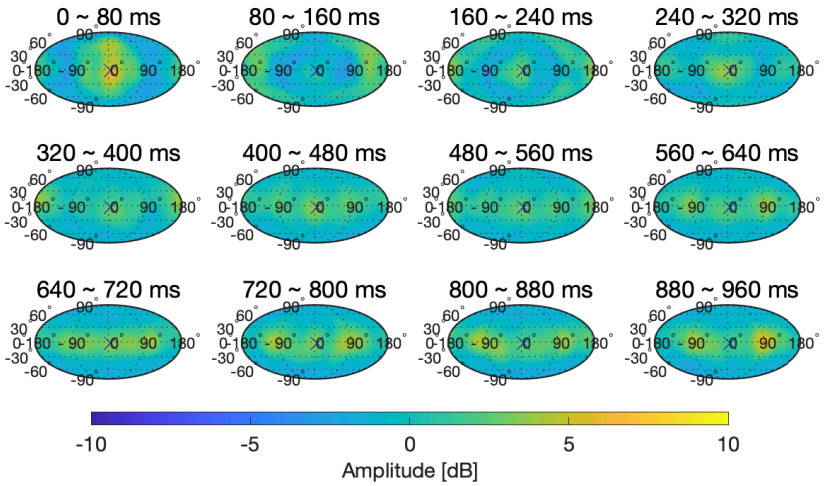

Figure 7: Condition D (Acoustic coefficient for all surface: 0.2, Sound source position: S1)

Therefore, decay cancellation would be useful for analyses with relatively long time window depending on purposes of the study. While its effect is limited in the current study employing 80 ms time window, the authors included the decay cancellation to the analysis method for enhancing its general versatility.

Furthermore, it should be noted that the decay cancellation is applicable only to impulse responses, which is the case in this study. For source signals that have a certain temporal duration, multiple direct and reflected sounds having different propagation delays are superimposed in room response signals. In such a case, therefore, the decay cancellation as in [7] and current study is not applicable.

7. Conclusion

In this paper, the relation between the DoA distribution in late reverberation and the properties of a room has been analyzed. The analysis from geometrical acoustic simulations was conducted. The results showed that the DoA distribution of late reverberation is biased toward a direction related to the acoustic

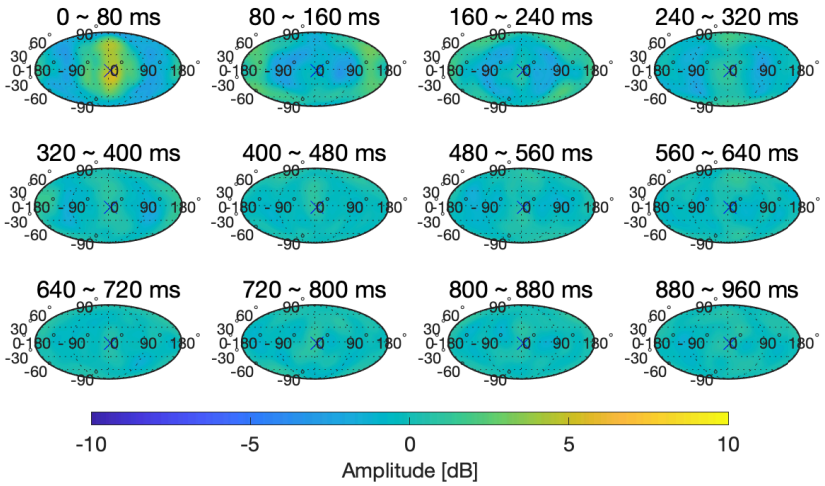

Figure 8: Condition E (Acoustic coefficient for all surface: 0, Sound source position: S1)

absorption and the shape of the room while sound source position does not affect the DoA distribution in late reverberation largely. Moreover, the results implies that the DoA distribution in late reverberation might be useful for analyzing acoustic characteristics of a room.

Acknowledgement

The authors would thank Prof. T. Tsuchiya, Doshisha Univ. and Mr. H. Okumura, Yamaha Corp. for their supports in the real measurement in Hardy Hall. This work was partially funded by JSPS Grants (Nos. 19H04153 and 19H04145).

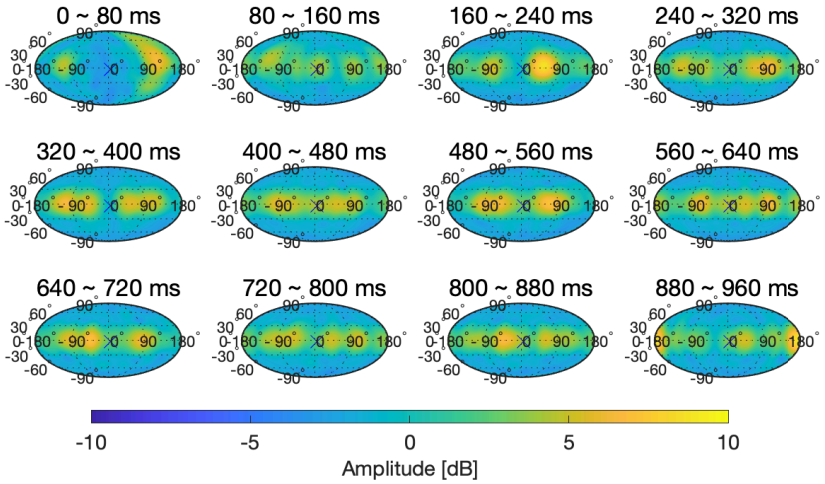

Figure 9: Condition F (Acoustic coefficient for the floor surface: 0.8, and that for the other surface: 0.2, Sound source position: S2)

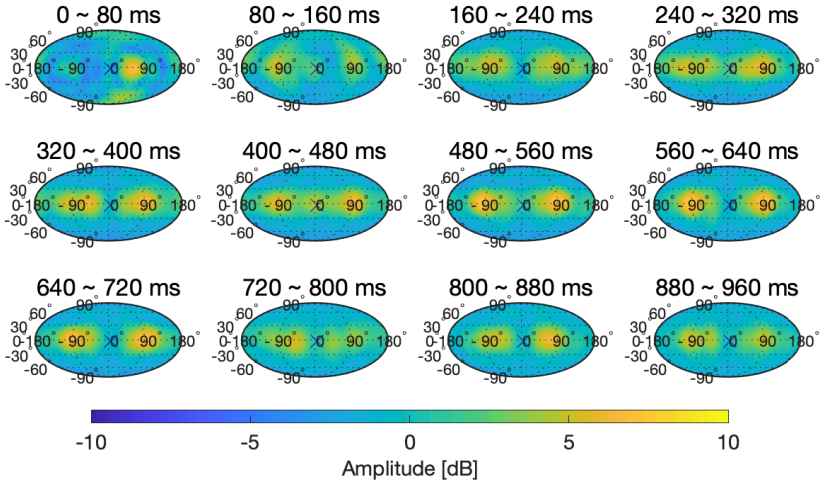

Figure 10: Condition G (Acoustic coefficient for the floor surface: 0.8, and that for the other surface: 0.2, Sound source position: S3)

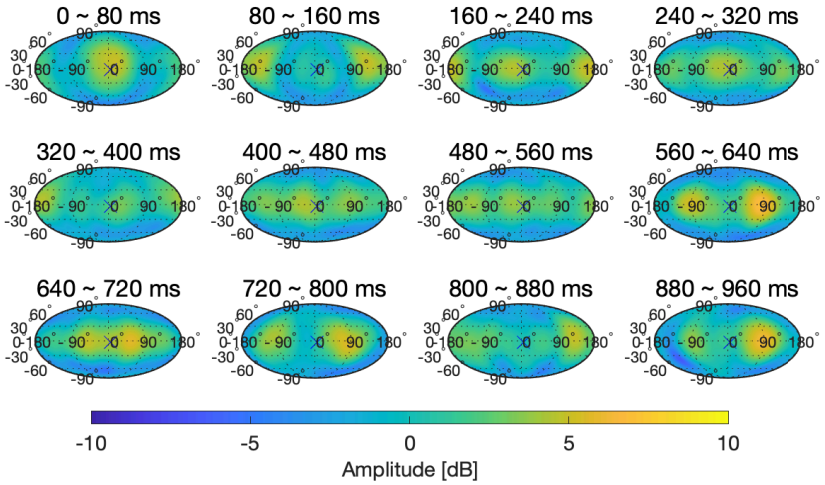

Figure 11: Condition A analized in 1,000 Hz octave band

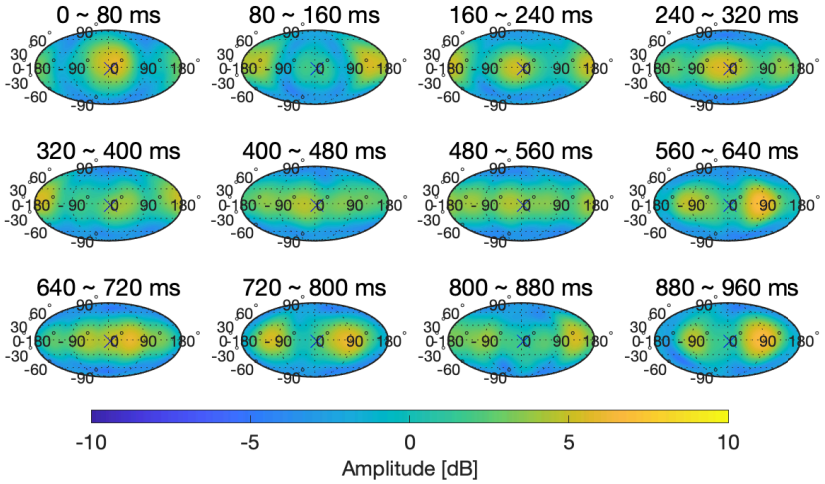

Figure 12: Condition A analized in 2,000 Hz octave band

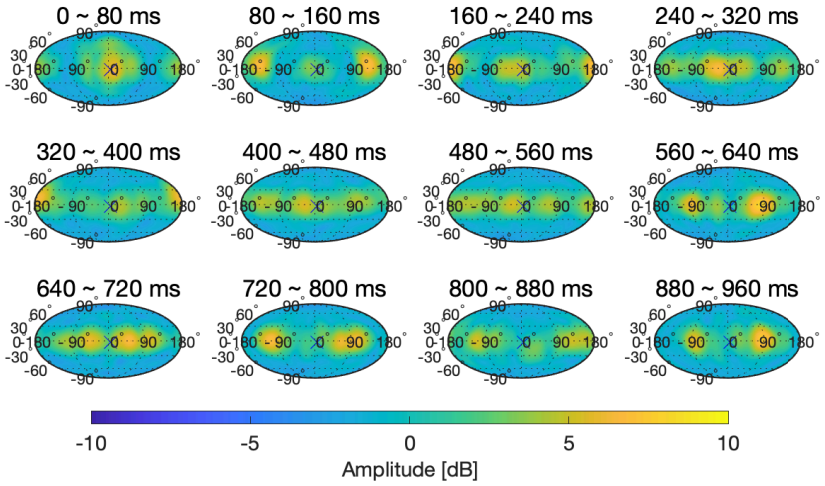

Figure 13: Condition A analized without decay cancellation (80 ms time window)

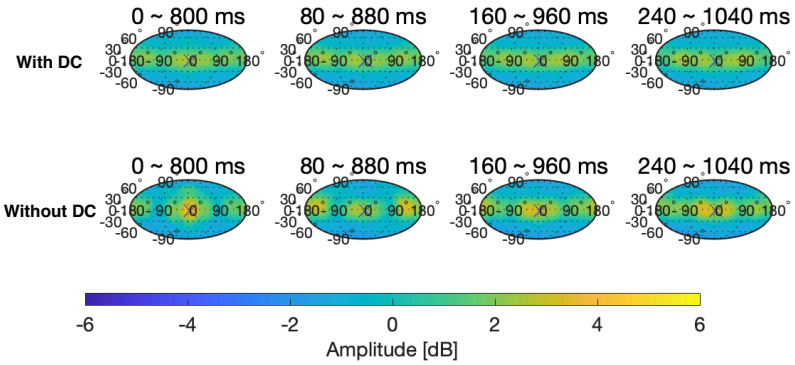

Figure 14: Condition A analized with (upper row) and without (lower row) decay cancellation (DC) (800 ms time window)

References

[1] T. Okano, L. L. Beranek, T. Hidaka, Relations among interaural cross-correlation coefficient ($IACC_E$), lateral fraction (LF_E), and apparent source width (ASW) in concert halls, The Journal of the Acoustical Society of America 104 (1) (1998) 255–265. doi:10.1121/1.423955.

[2] J. S. Bradley, G. A. Soulodre, The influence of late arriving energy on spatial impression, The Journal of the Acoustical Society of America 97 (4) (1995) 2263–2271. doi:10.1121/1.411951.

[3] T. Hanyu, S. Kimura, New objective measure for evaluation of listener envelopment focusing on the spatial balance of reflections, Applied Acoustics 62 (2) (2001) 155–184. doi:10.1016/S0003-682X(00)00054-2.

[4] W. Clement Sabine, Collected Papers on Acoustics, Tech. rep. (1921).

[5] C. F. Eyring, Reverberation Time in "Dead" Rooms, Journal of the Acoustical Society of America 1 (2A) (1930) 217–241. doi:10.1121/1.1915175.

[6] T. Hanyu, D. Inage, S. Katsuaki, Measurment of directional information of sound field by 4-channel cardioid microphones, in: Proceedings of the Spring Meeting, Acoustical Society of Japan, The Acoustical Society of Japan, 2008, pp. 1123–1126.

[7] R. Suzuki, K. Hoshi, T. Hanyu, Analysis of directional distribution of arriving sound energy using instataneous intensity and decay-cancelled impulse response, in: Summaries of technical papers of annual meeting Architectural Institute of Japan, Architectural Institute of Japan, 2014, pp. 251–252.

[8] M. Berzborn, M. Nolan, E. Fernandez-grande, M. Vorländer, On the Directional Properties of Energy Decay Curves, in: Proceedings of the 23rd International Congress on Acoustics, 2019, pp. 4043–4050.

[9] M. Vorländer, M. Berzborn, The Directional Energy Decay Curve in Performance Spaces, in: Proceedings of the International Symposium on Room Acoustics, 2019, p. 473.

[10] Y. Izumi, M. Otani, Direction-of-arrival distribution analysis of reflected sounds using spherical microphone array, in: Proceedings of the International Symposium on Room Acoustics, no. September, 2019, pp. 305–312.

[11] J. Meyer, G. Elko, A highly scalable spherical microphone array based on an orthonormal decomposition of the soundfield, in: IEEE International Conference on Acoustics, Speech, and Signal Processing, Vol. 2, 2002, pp. II1781–II1784. doi:10.1109/ICASSP.2002.5744968.

[12] B. Rafaely, Plane-wave decomposition of the sound field on a sphere by spherical convolution, The Journal of the Acoustical Society of America 116 (4) (2004) 2149–2157. doi:10.1121/1.1792643.

[13] M. Park, B. Rafaely, Sound-field analysis by plane-wave decomposition using spherical microphone array, The Journal of the Acoustical Society of America 118 (5) (2005) 3094–3103. doi:10.1121/1.2063108.

[14] F. H. de Araujo, F. A. d. N. Castro Pinto, J. C. Boscher Torres, Room reflections analysis with the use of spherical beamforming and wavelets, Applied Acoustics 131 (2018) 192–202. doi:10.1016/j.apacoust.2017.10.030.

[15] B. Rafaely, Analysis and design of spherical microphone arrays, IEEE Transactions on Speech and Audio Processing 13 (1) (2005) 135–143. doi:10.1109/TSA.2004.839244.

[16] T. Hanyu, Analysis Method for Estimating Diffuseness of Sound Fields by Using Decay-Cancelled Impulse Response, Building Acoustics 21 (2) (2014) 125–133. doi:10.1260/1351-010X.21.2.125.

[17] S. Kaneko, T. Suenaga, H. Akiyama, S. Sekine, A microphone array for 3-dimensional sound eld recording, based on the Fibonacci-spiral, in: Pro-

ceedings of the Autumn Meeting, Acoustical Society of Japan, The Acoustical Society of Japan, 2017, pp. 715–716.

[18] I. Dalenbäck, Bengt, TUCT TM v2.0a User's Manual CATT-Acoustic TM v9.1, Tech. rep. (2016).